Influence of plasticiser type and nanoclay on the properties of chitosan-based materials‡

Pei Chen [a,b], Fengwei Xie [b,*,†], Fengzai Tang [c], Tony McNally [b,**]

[a] *College of Food Science, South China Agricultural University, Guangzhou, Guangdong 510642, China*

[b] *International Institute for Nanocomposites Manufacturing (IINM), WMG, University of Warwick, Coventry CV4 7AL, United Kingdom*

[c] *WMG, University of Warwick, Coventry CV4 7AL, United Kingdom*

[*] Corresponding author. Email addresses: d.xie.2@warwick.ac.uk, fwhsieh@gmail.com (F. Xie)

[**] Corresponding author. Email address: t.mcnally@warwick.ac.uk (T. McNally)

[†] This author leads the research.

‡ Supplementary material provided.

Abbreviations: MMT, montmorillonite; CMC, carboxymethyl cellulose; IL, ionic liquid; [C_2mim][OAc], 1-ethyl-3-methylimidazolium acetate; PEC, polyelectrolyte complexation; T_d, thermal decomposition temperature at maximum weight-loss rate; tan δ, loss tangent; T_β, peak temperature of β-transition; T_α, peak temperature of α-transition; E, Young's modulus; σ_t, tensile strength; ε_b, elongation at break; θ_{c0s}, contact angle at 0 s; θ_{c60s}, contact angle at 60 s; RH, relative humidity; RT, room temperature.

Abstract:

Chitosan, a biocompatible polysaccharide having antimicrobial efficacy, is highly useful for biomedical and other applications. How chitosan properties can be tailored continues to attract intense research interest. Herein, chitosan and chitosan/carboxymethyl cellulose (CMC) materials filled with montmorillonite (MMT) were thermomechanically processed resulting in excellent nanoclay dispersion. Inclusion of MMT significantly increased the molecular relaxation temperatures, tensile mechanical properties, and film surface hydrophobicity. When plasticisers such as 1-ethyl-3-methylimidazolium acetate ([C_2mim][OAc]) or glycerol were introduced, the effect of MMT on the biopolymer properties largely depends on whether the MMT alters plasticiser–biopolymer interactions. [C_2mim][OAc]-plasticised chitosan exhibited a relatively high contact angle (100±7°) similar to the un-plasticised chitosan/MMT material, derived from the strong hydrogen-bonding capability of [C_2mim][OAc]. Polyelectrolyte complexation (PEC) allowed the glycerol-plasticised chitosan/CMC material to have a hydrophobic surface (contact angle: 90±6°) similar to that of the un-plasticised chitosan/CMC/MMT material. Specifically, further inclusion of MMT interrupted biopolymer–plasticiser interactions, leading to increased surface wettability. However, while addition of [C_2mim][OAc] resulted in reduced hydrophilicity of the chitosan/CMC matrix, addition of MMT counteracted this effect by interacting with the IL. This work shows the plasticizers and MMT influence surface hydrophilicity mainly by determining the availability of free biopolymer polar groups.

Keywords: Biopolymer thermomechanical processing; Polysaccharide plasticisation; Chitosan nanocomposites; Nanoclay; Ionic liquid; Surface hydrophilicity

1 Introduction

The utilisation of natural biopolymers such as polysaccharides (*e.g.* cellulose, chitin/chitosan, starch, and alginate) and proteins continue to attract increasing interest as these materials are renewable, are widely available, biodegradable, and have low toxicity or are non-toxic. For the production of products, biopolymers are usually processed with plasticisers since, without plasticiser, biopolymer materials are too brittle or fragile to use [1]. Glycerol is the most widely used plasticiser for biopolymers due to its non-volatility and matching hydrophilicity. In recent years, ionic liquids (ILs) have attracted much attention for the processing and plasticisation of biopolymers, especially starch [2-10]. ILs that contain a strongly basic, hydrogen-bond-accepting anion (*e.g.* carboxylates or halides) can effectively disrupt biopolymer hydrogen-bonded networks [10].

However, how biopolymer–plasticiser (especially IL) interactions determine the properties of biopolymers is not fully understood. Chen et al. [11] suggested that glycerol is more advantageous for chitosan plasticisation than ILs because the hydrophobic end groups (C─H) of glycerol can prevent hydrogen bonding between chitosan chains whereas ILs, which have stronger hydrogen-bonding capability, can form multiple hydrogen bonds with chitosan chains and thus limit chain mobility. In contrast, a few studies [2, 4, 6, 7, 12] indicated that ILs are more effective plasticisers than glycerol for biopolymers such as starch, protein, and chitosan, resulting in a more amorphous structure, greater chain mobility, and mechanical ductility. Moreover, while ILs are more hydrophilic than glycerol, there has been no consensus on how plasticisers affect the hydrophilicity or hygroscopicity of biopolymers. Sankri et al. [6] indicated that starch plasticised by 1-butyl-3-methylimidazolium acetate ([C_4mim]Cl) were significantly less hygroscopic than the glycerol-

plasticised counterpart. Zhang et al. [4] found that at a high plasticiser content (24 wt%), starch plasticised by 1-ethyl-3-methyl-imidazolium acetate ([C_2mim][OAc]) showed greater water uptake during conditioning at 75% relative humidity (RH), whereas the reverse was observed at a low plasticiser content (9 wt%).

Nanocomposites from biorenewable resources have been produced to enhance mechanical properties (tensile, flexural, and impact) and play a wide and increasing role in diverse industrial applications (e.g. drug delivery, tissue engineering, fuel cells, electronics, food packaging, environmental remediation, genetic engineering, and biomedical sciences) [13]. Nonetheless, limited studies have been undertaken on how nanofillers influence the hydrophilicity of plasticised biopolymers other than starch. In the area of starch-based nanocomposites, it has been established that the hydrophilic nature of glycerol can negate the improved water resistance provided by montmorillonite (MMT) [14]. In a study [15] where chitosan was shown to function as a compatibiliser between the starch matrix and MMT, higher chitosan content led to increased surface hydrophobicity and decreased water vapour transmission rate and moisture absorption of the composite film. MMT was also found to decrease the water absorption, water solubility, and surface wettability of carboxymethyl starch films [16]. In these studies, the increased hydrophobicity was attributed to the biopolymer–MMT interaction and the tortuous path in the matrix created by the delaminated 2D nanoclay. However, how the interplay between nanofiller and plasticiser affects the surface hydrophilicity of chitosan-based nanocomposites has largely been unexplored, which forms the motivation for this current study.

We prepared chitosan and chitosan/carboxymethyl cellulose (CMC) polyelectrolyte-complexed materials with MMT by thermomechanical processing. This method provides strong shear stresses and efficient mixing for high filler concentration and high-viscosity 'melts', enabling excellent dispersion of MMT nanosheets in the biopolymer matrices as well as the plasticisation of biopolymers [17-21]. This method could also realise macroscopically uniform, bulky polyelectrolyte-complexed biopolymer materials, whereas in frequently used solution conditions, the rapid complexation between two polymers at the contact interface can result in heterogeneous aggregates [22]. We hypothesise that the material surface hydrophilicity/hydrophobicity can be largely influenced by the varying biopolymer–plasticiser interactions, while mechanical properties are mainly controlled by biopolymer inter-chain hydrogen bonding. We propose mechanisms underlying the hydrophilicity/hydrophobicity of biopolymer materials that were affected by MMT and the plasticisers ([C_2mim][OAc] and glycerol).

2 Materials and methods

2.1 Materials

Chitosan (poly(β-(1,4)-D-glucosamine), derived from crab shells, with a viscosity of about 100 mPa·s (*i.e.* 1% solution in 1% acetic acid at 25 °C), a degree of deacetylation of >90%, and a weight-average molecular mass (M_w) of about 150k g·mol^{-1}, was purchased from Shanghai Ryon Biological Technology Co., Ltd (China). This chitosan was characterised previously [23]. CMC sodium, with a viscosity of 50–100 mPa·s (Brookfield, 2% solution, at 25 °C), a degree of substitution (DS) of 0.7, and an M_w value of 90,000 g·mol^{-1}, was acquired from Shanghai Macklin Biochemical Co., Ltd (China). The characteristics of this CMC were reported in our previous study [24]. Glycerol (≥99%

analytical grade) was supplied by Fisher Scientific UK Ltd (UK); [C_2mim][OAc] (≥95.0%) and MMT K 10 (surface area 220–270 m^2/g) by Sigma-Aldrich Company Ltd (UK); formic acid (98 wt% AR) and NaBr (pure) by Scientific Laboratory Supplies Ltd (UK). Deionised water was used throughout.

2.2 Sample preparation

Table 1 shows the formulations and corresponding codes of the different chitosan-based samples prepared in this study. The matrices used were either chitosan alone (A) or chitosan/CMC (B). The codes also indicate the plasticiser used, with, for example, "G2" representing 20 wt% glycerol and "E4" indicating 40 wt% [C_2mim][OAc]. The suffix "F" denotes the samples were prepared as films. Following our method established previously [24], the samples were prepared by pre-blending the ingredients, thermomechanical kneading at 80 °C for 15 min, hot-pressing at 110 °C and 160 bar for 10 min, and conditioning at 57% RH for three weeks before characterisation. The samples without plasticiser or MMT (A-F and B-F) [24], those plasticised by glycerol without MMT (AG2-F, AG4-F, BG2-F, and BG4-F) [25], and those plasticised by [C_2mim][OAc] without MMT (AE2-F, AE4-F, BE2-F, and BE4-F) [26], all prepared in the same way, have been reported previously and are used for comparison throughout the discussion.

Table 1. Sample codes and compositions (represented as portions by weight).

Sample	Chitosan	CMC	Glycerol	$[C_2mim][OAc]$	MMT	2M Formic acid solution
A/M-F	100	–	–	–	0.75	261
AG2/M-F	100	–	20	–	0.75	261
AG4/M-F	100	–	40	–	0.75	261
AE2/M-F	100	–	–	20	0.75	261
AE4/M-F	100	–	–	40	0.75	261
B/M-F	50	50	–	–	0.75	261
BG2/M-F	50	50	20	–	0.75	261
BG4/M-F	50	50	40	–	0.75	261
BE2/M-F	50	50	–	20	0.75	261
BE4/M-F	50	50	–	40	0.75	261

2.3 Sample characterisation

Scanning electron microscopy (SEM) imaging was performed using a ZEISS SIGMA field-emission scanning electron microscope with an acceleration voltage of 6 kV. The biopolymer films were cryo-fractured using liquid nitrogen and the samples sputter-coated with gold/palladium before imaging.

Scanning transmission electron microscopy (STEM) was conducted using a Talos F200X transmission electron microscope at 200 kV to obtain both bright-field (BF) and high-angle annular dark-field (HAADF) images. Ribbons about 60 nm thick were sectioned from epoxy-embedded sample blocks and subsequently transferred onto holey carbon films on 200-mesh copper grids. No liquid was used during preparation to avoid damaging the samples.

X-ray diffraction (XRD) analysis was undertaken using a PANalytical Empyrean X-ray diffractometer at 40 kV and 40 mA with a Co target (Kα = 1.790307 Å) and a beam slit of 10 mm. The samples were scanned over an angular range (2θ) of 6–40° with a step size of 0.0263° and a step rate of 2.16 s/step.

Fourier-transform infrared (FTIR) spectra were collected using a Bruker TENSOR 27 FTIR spectrometer with an attenuated total reflection (ATR) accessory with 32 scans for each sample over a range of 4000–500 cm^{-1} at room temperature (RT).

Thermo-gravimetric analysis (TGA) was undertaken using a Mettler Toledo TGA apparatus over a temperature range of 30–700 °C at 10 K/min under nitrogen.

Dynamic mechanical thermal analysis (DMTA) was performed using a Tritec 2000 DMA (Triton Technology Ltd., UK) in the dual cantilever mode with a sample length of 5 mm at a displacement of 0.01 mm. Temperature scans were performed from −100 °C to 180 °C at 2 K/min and 1 Hz. The dynamic storage modulus (E'), loss modulus (E''), and loss tangent ($\tan \delta = E''/E'$) were automatically calculated by the software.

Tensile tests were performed using an Instron 3367 universal testing machine with a 1kN load cell at a crosshead speed of 3 mm/min. As the specimens were in the form of thin sheets, specimen extension was measured by grip separation as recommended by ASTM Standard D882. Young's modulus (E), tensile strength (σ_t), and elongation at break (ε_b) were automatically determined using Instron Bluehill 3 software from at least seven replicates for each sample.

Contact angle data were obtained from sessile tests at RT based on Young–Laplace using an Attension Theta Lite instrument (Biolin Scientific, UK). As the contact angle kept changing after the

water drop was placed on the biopolymer film surface, contact angles at 0 s and 60 s (θ_{c0s} and θ_{c60s}, respectively) were recorded.

3 Results and Discussion

3.1 Morphology and structures of chitosan-based composites

Figure S1 shows SEM images of cryo-fractured surfaces of the different bionanocomposite films. All the samples displayed a cohesive structure, indicating successful processing of chitosan and CMC. No significant difference in micron-scale morphology can be seen between these MMT-filled and unfilled biopolymers (*i.e.* without MMT) [24-26].

Figure 1 shows the morphology of neat MMT imaged using STEM. Stacks or agglomerations of large and individual sheets of MMT can be seen. In some areas, the MMT is just a few layers thick and was seen to be translucent, whereas the creases in the stacks had greater contrast and were more visible.

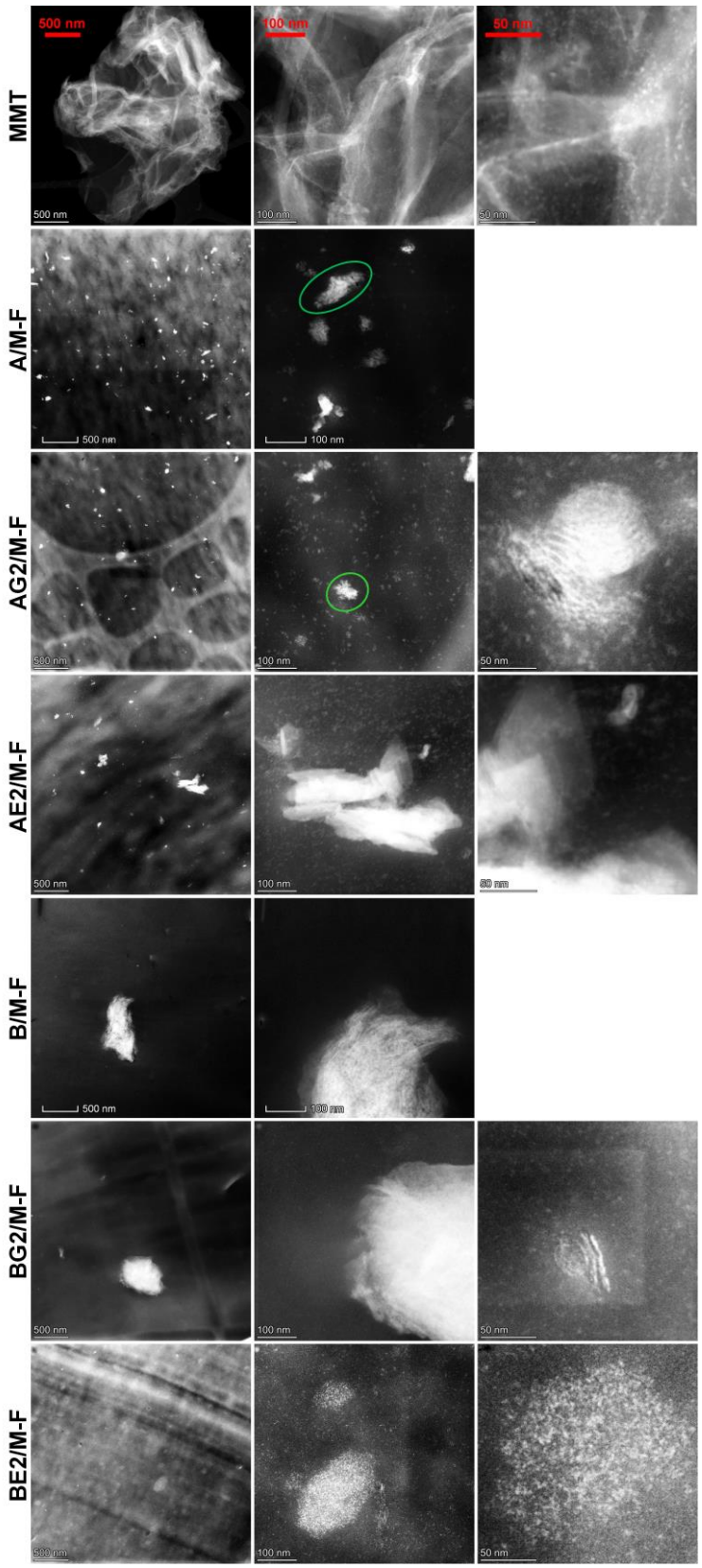

Figure 1. Scanning transmission electron microscopy high-angle annular dark-field (STEM-HAADF) images of MMT and the different bionanocomposite films. Green circles indicate possible un-processed chitosan structure.

STEM was also used to examine the different bionanocomposite films, also shown in **Figure 1**. For all the A-series of bionanocomposites, many bright dots in HAADF images can be seen (examples enclosed by green circles), which are also exhibited by A-F [24]. These dots could be some unprocessed chitosan structure. As no other features apparently existed in A/M-F, we consider MMT was predominately delaminated and became invisible especially against the chitosan background under STEM. MMT is naturally negatively charged because of isomorphic substitutions occurring between clay platelets [28, 29]. As a result, a strong affinity between chitosan and MMT should be expected because of not only the matching hydrophilicity but also ionic interaction, leading to the intercalation of chitosan chains between MMT platelets and the subsequent delamination of MMT platelets. In previous studies [17, 30], where significantly higher amounts (2.5–10 wt%) of MMT were incorporated into chitosan, features like the creases or waviness of MMT stacks were apparent and ubiquitous in the nanocomposites.

Compared with A/M-F, the images for AG2/M-F and AE2/M-F revealed some MMT agglomerations. They also showed some ‘cloudy’ areas with diffused bright contrast in the HAADF images, indicative of a “dissolvable” feature, which, may be ascribed to partially exfoliated MMT nanosheets. Thus, the plasticiser negatively affected the delamination of MMT as it competed with the biopolymer to interact with the MMT. However, as these agglomerations or ‘cloudy’ areas are small in number and scattered distantly, it is considered that most of the MMT nanosheets were still well dispersed in the chitosan matrix because of the strong shearing action applied during processing, and the single and small bundles of nanosheets became much less visible.

B/M-F is similar to B-F [24], except that some MMT agglomerations were visible, larger than those in A/M-F. In this regard, the ionic and hydrogen-bonding interactions between CMC and chitosan may have competed with the similar interactions between chitosan and MMT, leading to poorer MMT dispersion in the polyelectrolyte-complexed chitosan/CMC (B) matrix. BG2/M-F also contained large agglomerations of MMT as well as 'dissolvable' features. Different from other samples, BE2/M-F displayed large densely populated structures. As BE2-F did not show this morphology [26], these features may be ascribed to partially exfoliated MMT nanosheets. In BE2/M-F, the IL (especially $[C_2mim]^+$ cation) may have interacted with MMT through ionic interaction, contributing to the dispersion of MMT nanosheets. This phenomenon is worth further investigation.

Figure 2 shows the FTIR spectra for the different bionanocomposites. Our previous studies [25, 26] indicated that, for the A-matrix, plasticisation by glycerol could cause blue shifts of the absorption bands originally at 1572 cm^{-1} (N─H bending from amine and amide II) and 1022 cm^{-1} (skeletal vibration of C─O stretching). For the B-matrix, inclusion of glycerol also caused a blue shift of the absorption band at 1022 cm^{-1} and no significant changes to peak position were observed for the A- and B-matrices plasticised by $[C_2mim][OAc]$. Complexation between chitosan and CMC caused a blue shift of the absorption band at 1572 cm^{-1} and a red shift of the band at 1065 cm^{-1} (asymmetric C─O─C stretching in the glycosidic linkage), suggesting strong molecular interactions between chitosan and CMC [25, 26]. MMT displayed a sharp peak at 1001 cm^{-1} (**Figure S2**) due to the Si─O silica stretching mode [31] and this characteristic band of MMT was still slightly visible for all the samples. Besides, some changes to the FTIR spectra caused by inclusion of MMT were obvious. Compared with that for A-F and B-F, for A/M-F and B/M-F the band at 1065 cm^{-1} was red-

shifted and became less sharp. Compared with AE2-F and AE4-F, AE2/M-F and AE4/M-F displayed a slight blue shift of the band at 1022 cm^{-1}. For BG2/M-F, the band at 1022 cm^{-1} was also blue-shifted compared with that for BG2-F. In this regard, interaction of MMT with the biopolymers could have affected the biopolymer backbone chain and the saccharide ring by a steric hindrance effect.

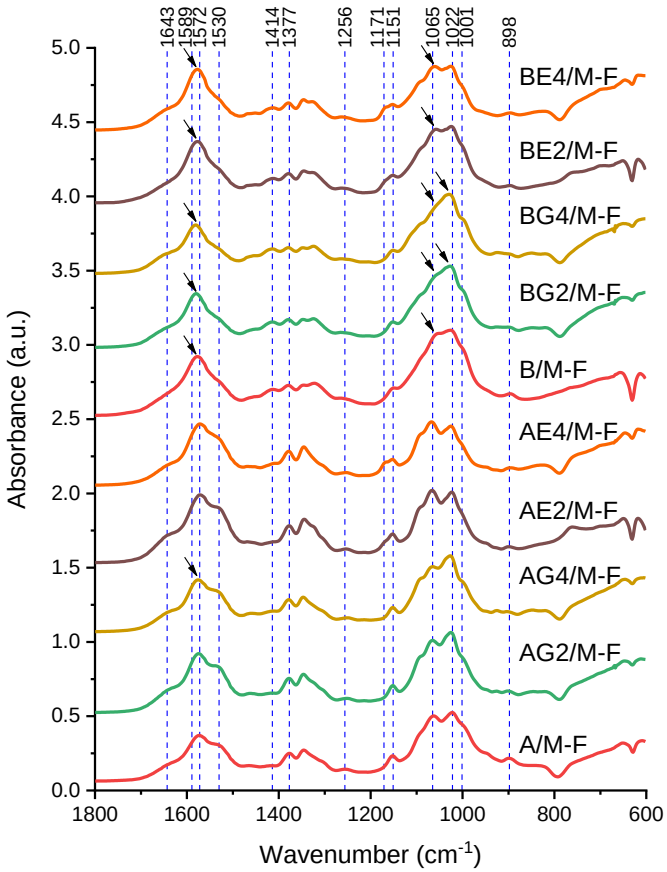

Figure 2. Fourier-transform infrared (FTIR) spectra for the different bionanocomposite films. The reference lines indicate characteristic bands for unprocessed CMC (1589, 1414 and 1022 cm^{-1}), unprocessed chitosan (1643, 1572, 1530, 1377, 1256, 1151, 1065, 1022 and 898 cm^{-1}) [24], [C_2mim][OAc] (1171 cm^{-1}) [26], and MMT (1001 cm^{-1}) (**Figure S2**). The arrows indicate shifts in peak position or changes in peak intensity.

Figure 3 shows the XRD curves for the different bionanocomposites. As discussed previously [25, 26], the A-series of samples displayed an apparent crystalline structure, which should be predominantly due to re-crystallisation as their XRD patterns are completely different from that of unprocessed chitosan. The B-series of samples, un-plasticised or plasticised by glycerol, were largely amorphous, implying the complexation with CMC suppressed the re-crystallisation of chitosan. The B-series of samples plasticised by [C_2mim][OAc] had a low degree of crystallinity due to the re-crystallisation of chitosan facilitated by the IL. Inclusion of MMT to the different matrices did not result in changes to the XRD patterns for most samples. However, A/M-F showed reduced peak intensities relative to A-F, and B/M-F was more amorphous than B-F. This suggests that inclusion of MMT hindered the chain interactions and rearrangement for un-plasticised chitosan. Nonetheless, addition of 20 wt% glycerol allowed the chitosan chains to have greater mobility and therefore more likely to allow chain rearrangement and re-crystallisation especially with the assistance of MMT, as shown by AG2/M-F displaying more intense peaks than AG2-F. With these exceptions, the remaining MMT-filled biopolymers did not show XRD patterns different from those for the unfilled biopolymers.

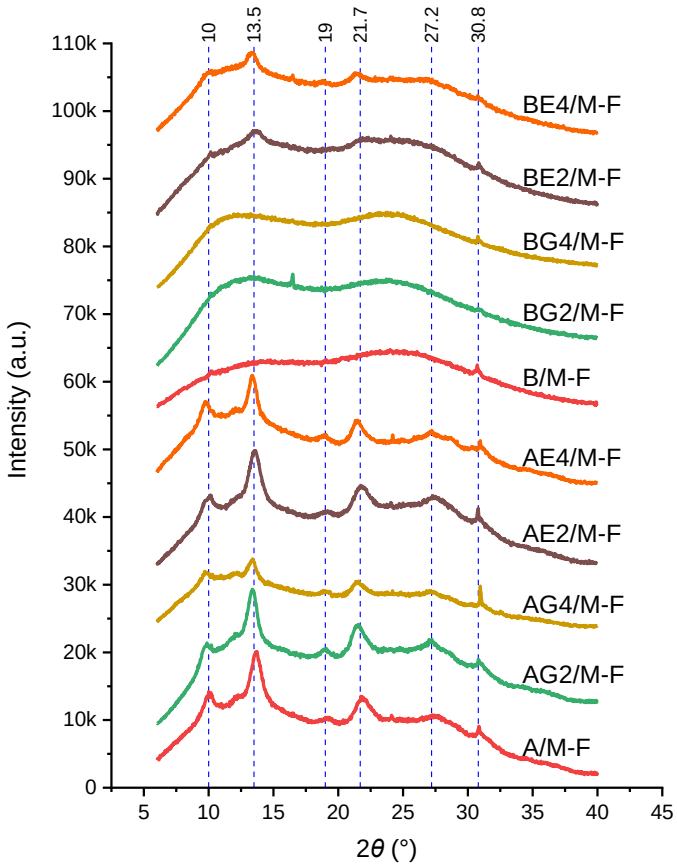

Figure 3. X-ray diffractograms for the different bionanocomposite films. The reference lines indicate characteristic peaks for A-F [24].

3.2 Material properties of chitosan-based composites

Figure 4 shows the curves of derivative weight as a function of temperature for the different bionanocomposites obtained by TGA. Compared with A-F where the major peak temperature (T_d, maximum weight-loss rate) was 296 °C [24], A/M-F was less thermally stable (T_d = 288 °C), perhaps associated with reduced chain interactions and crystallinity (discussed in XRD results). For the A-matrix plasticised by glycerol (20 wt% or 40 wt%), inclusion of MMT did not change T_d (284 °C for AG2/M-F and 262°C for AG4/M-F). AE2/M-F had a higher T_d value (278 °C) than that of AE2-F (272 °C) [26]. In this regard, while plasticisation by [C_2mim][OAc] significantly decreased the

thermal stability of chitosan, MMT counteracted this effect of the IL by shielding against the transfer of pyrolysis products [32]. However, for the chitosan matrix plasticised by the higher content (40 wt%) IL, which displayed further reduced thermal stability [26], the effect of MMT was insignificant (T_d = 256 °C for AE4/M-F).

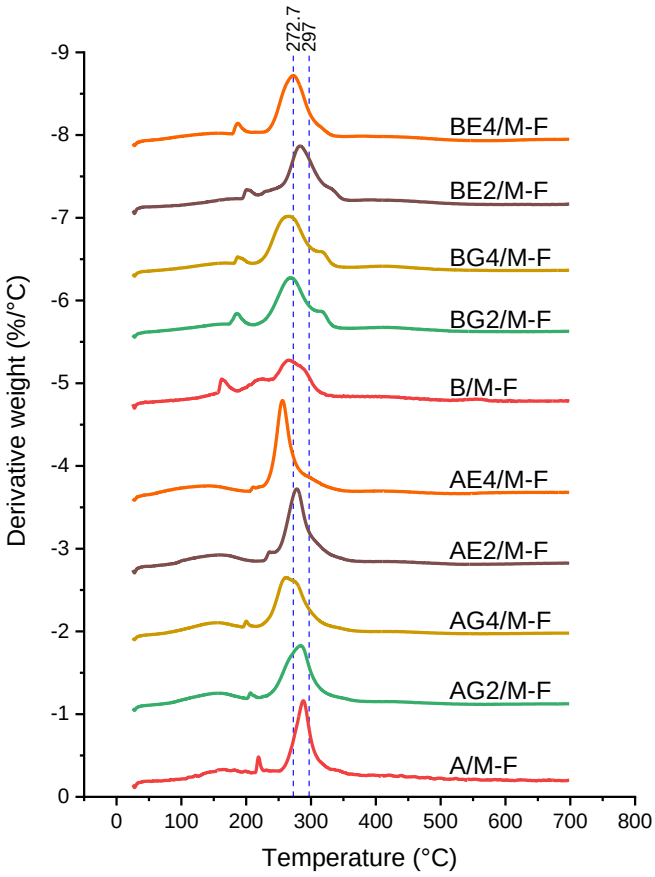

Figure 4. Derivative weight *vs.* temperature curves measured by thermogravimetric analysis (TGA) for the different bionanocomposite films. The reference lines indicate the major peak temperatures of A-F and B-F, respectively [24].

Our previous study [24] showed that B-F had a major weight loss as overlapped peaks at 273 °C (T_d) and 306 °C, along with small peaks at 169 °C and 223 °C associated with the initial de-

polymerisation of the biopolymers. The overlapped peaks at higher temperature (306 °C) may be attributed to the more thermally stable polyelectrolyte complexes. For B/M-F, T_d reduced to 266 °C and the peak derived from the polyelectrolyte complexes was less apparent. This corresponds with the reduction in crystallinity (see XRD results) and may also be derived from the partially weakened PEC between the two biopolymers due to the dispersed MMT nanosheets. BG2/M-F, BG4/M-F, BE2/M-F, and BE4/M-F had T_d values (269 °C, 265 °C, 283 °C, and 273 °C, respectively) similar to their respective matrix counterparts [25, 26], suggesting inclusion of MMT was ineffective at changing the thermal stability of these plasticised B-matrices. The high thermal stability of BE2/M-F is due to the enhanced chain interactions and re-crystallisation induced by [C_2mim][OAc].

Figure 5 shows the tan δ curves as a function of temperature measured by DMTA for the different bionanocomposites. For A-F, two transitions can be identified [24], a weak one centred at −47 °C associated with a β-relaxation of chitosan (the motions of the side chains or lateral groups of chitosan) and a much more prominent one at about 119 °C attributed to the α-transition (glass transition) of chitosan [33, 34]. For A/M-F, the peak temperature of the β-transition (T_β) increased to about −38 °C whereas the peak temperature of the α-transition (T_α) was 109 °C. Thus, for the un-plasticised A-matrix, inclusion of MMT restricted the movement of chitosan side chains, due to interaction between negatively charged MMT and the chitosan cation. For the plasticised A-matrix, inclusion of MMT did not result in changes to T_β or T_α. On the other hand, B-F also exhibited two major transitions (T_β = −43 °C and T_α = 97 °C) [24]. In comparison, B/M-F showed significantly higher relaxation temperature (T_β = −13 °C and T_α = 123 °C) indicating MMT restricted the mobility of both the side and main chains of the biopolymers in this ternary system. For the plasticised B-

matrix, inclusion of MMT did not significantly alter T_β or T_α. Therefore, biopolymer chain mobility in these composites is mainly determined by the plasticiser type. BE2/M-F had $T_\beta = -21$ °C and $T_\alpha =$ 93 °C, higher than the respective values for other plasticised B-samples [25, 26]. In this case, [C_2mim][OAc] enhanced inter-chain interactions rather than providing a plasticisation effect, in agreement with the high crystallinity and thermal stability discussed above.

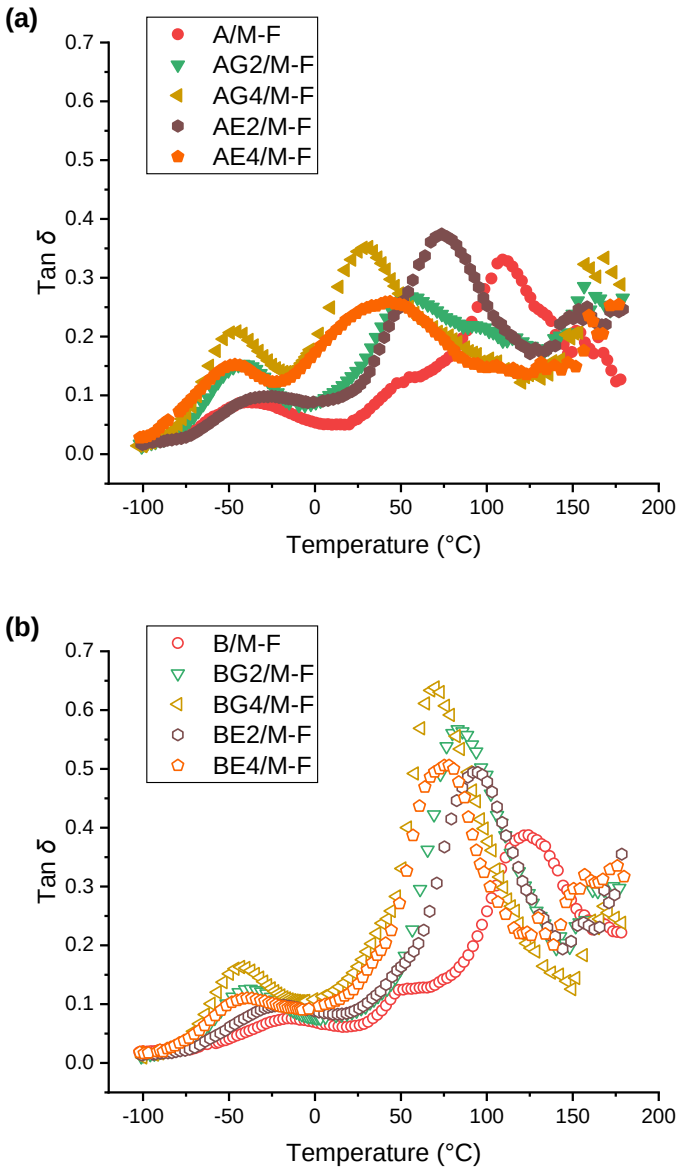

Figure 5. Dynamic mechanical thermal analysis (DMTA) results for the different bionanocomposite films.

Representative stress–strain curves from tensile testing (**Figure S3**) indicate that while AG4/M-F and AE4/M-F were more elastomeric, most samples behaved like a hard and tough polymer displaying strain-hardening behaviour. In particular, A/M-F, B/M-F, and BE2/M-F showed higher stiffness and strength, associated with the formation of an inter-chain hydrogen-bonded network in these samples. From the stress–strain curves, the calculated E, σ_t, and ε_b values are shown in **Figure 6** (a), (b) and (c), respectively. Compared with A-F (E = 1260±169 MPa, σ_t = 46.8±5.6 MPa, and ε_b = 22.6±4.6%), A/M-F displayed significant increases in these mechanical properties (E = 1744±118 MPa, σ_t = 60.4±1.1 MPa, and ε_b = 13.1±2.9%). Compared with B-F (σ_t = 50.5±3.6 MPa, and ε_b = 10.4±3.4%), B/M-F had higher σ_t (68.4±5.9 MPa) and ε_b (13.1±2.8%). The enhanced mechanical properties of the composites where MMT was added to the A- and B-matrices can be ascribed to the strong hydrogen-bonding and electrostatic interactions between MMT and chitosan and the large surface areas of MMT nanosheets, both contributing to effective stress transfer, despite the lower crystallinity (see XRD results) and possible decreased chitosan chain interactions, as discussed above. B/M-F also exhibited higher σ_t than A/M-F while both samples had similar ε_b, behaviour derived from PEC and an enhanced hydrogen-bonded network.

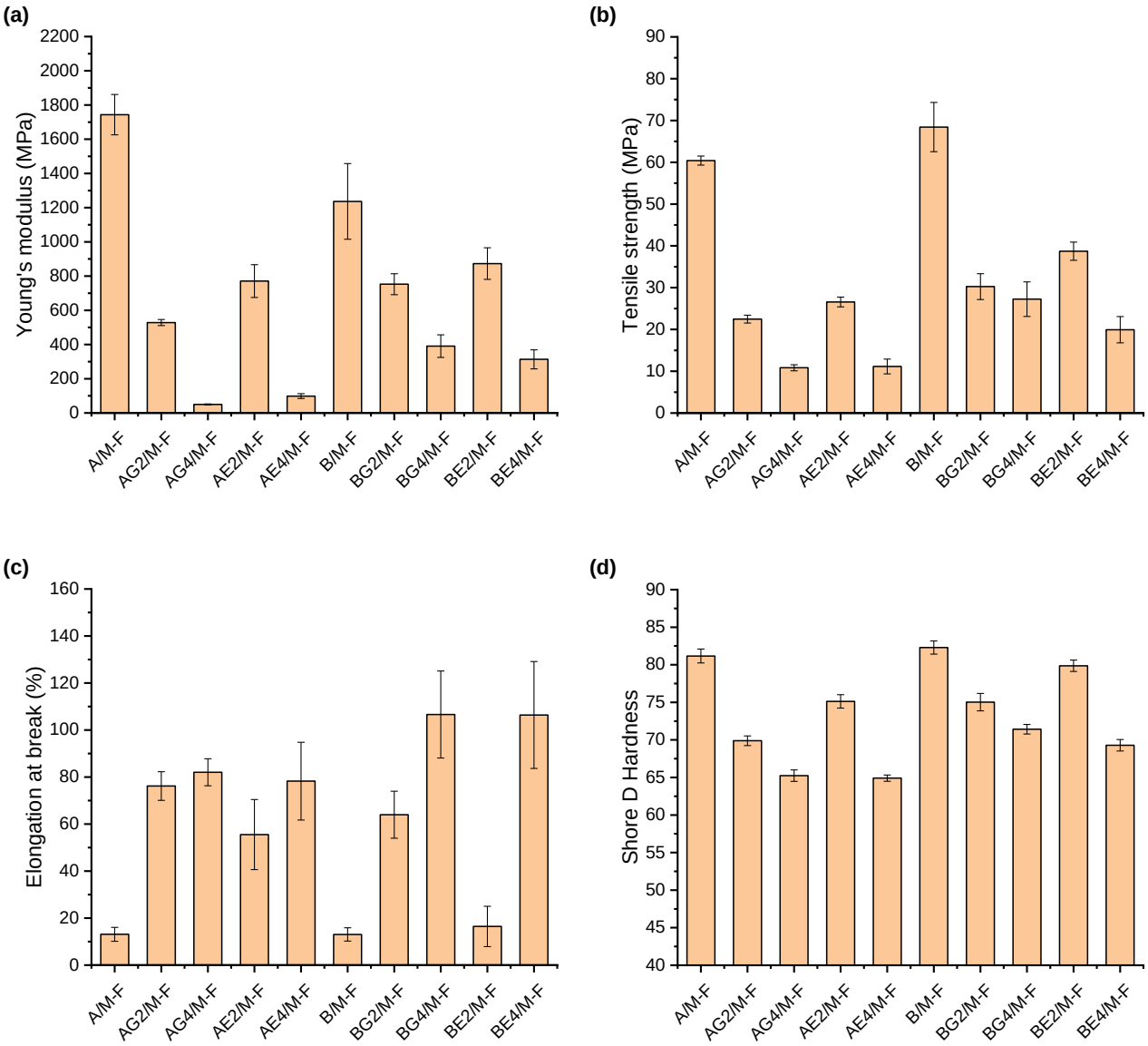

Figure 6. Tensile properties (a) Young's modulus, b) tensile strength and c) Elongation at break) and d) Shore D hardness for the different bionanocomposite films. Error bars represent standard deviations.

However, when the A- or B-matrix was plasticised with 20 wt% glycerol, inclusion of MMT even resulted in poorer mechanical properties. Specifically, AG2/M-F had E = 528±18 MPa and σ_t = 22.5±0.9MPa, lower than those for AG2-F (E = 730±26 MPa and σ_t = 26.3±1.4 MPa) [25]. BG2/M-F had E = 528±18 MPa and σ_t = 22.5±0.9MPa, lower than those for BG2-F (E = 883±65 MPa and σ_t =

38.4±2.8 MPa) [26]. In AG2/M-F and BG2/M-F, the inclusion MMT may assist the distribution of glycerol in the chitosan matrix and promote interactions with the biopolymer. While AG2/M-F had moderately higher crystallinity than AG2-F (see XRD results), crystallinity seemingly did not play a dominant role in determining the mechanical properties. A higher content (40 wt%) of glycerol resulted in weaker biopolymer chain interactions and in this case, MMT may assist with limited stress transfer between biopolymer chains. Therefore, AG4/M-F exhibited marginally higher σ_t (10.8±0.7 MPa) and ε_b (82.0±5.7%) than AG4-F (σ_t = 8.5±0.5 and ε_b = 58.8±5.1%) [25]. BG4/M-F had a slightly higher E value (391±66 MPa) than BG4-F (333±60 MPa) [25].

For the A-matrix plasticised by [C_2mim][OAc], inclusion of MMT did not result in significant changes in the mechanical properties of chitosan, except that AE2/M-F had lower ε_b (55.5±15.0%) than AE2-F (72.0±9.2%) [26]. This shows the dominant role of the plasticiser in determining the interactions between chitosan chains, whereas the interaction between chitosan and MMT was weak. Due to ionic interactions, the [C_2mim]$^+$ cation is likely to bind with the MMT. On the other hand, BE2/M-F displayed lower ε_b (16.4±8.6%) than BE2-F (33.4±8.0%) [26], and BE4/M-F showed lower E (333±56 MPa) and σ_t (19.9±3.1 MPa) than BE4-F (E = 518±82 MPa and σ_t = 24.0±3.2%) [26]. Likely, in the B-matrix plasticised by [C_2mim][OAc], MMT could restrict inter-chain hydrogen bonding. This will be further discussed in Section 3.3.

Figure 6 d) shows the Shore D hardness for the different samples, which shows similar trends shown by E and σ_t from tensile testing. In the regard, the plasticisers and inclusion of MMT influenced the hardness in the same way as for tensile properties. The highest Shore D hardness was obtained for A/M-F (81.2±0.9) and B/M-F (82.3±0.9). The hardness values for the two MMT-filled

345 un-plasticised samples were higher than that for the respective unfilled matrices (77.2±0.9 for A-F
346 and 77.5±0.9 for B-F), suggesting reinforcement is derived from the MMT. Compared with A-F and
347 A/M-F, all plasticised A-samples showed lower hardness values irrespective of MMT addition.
348 Compared with B-F, only BG2-F, BE2-F, and BE2/M-F displayed higher hardness values but still
349 lower than that of B/M-F. Overall, plasticisation had a greater effect than MMT addition on
350 biopolymer material hardness.

351 The surface wettability (hydrophilicity/hydrophobicity) of materials is important particularly for
352 biomedical applications requiring biocompatibility and cell adhesion [35]. Cell adhesion occurs
353 preferentially on moderately water-wettable polymer surfaces [36]. In addition, high surface
354 hydrophilicity can lead to a hydrated layer on the materials as a high-surface-energy barrier to
355 prevent biofouling (protein absorption) [37]. Therefore, it is interesting to tailor the surface
356 wettability of chitosan materials via plasticisation or nanofiller addition. **Figure 7** shows the contact
357 angle values obtained showing the surface hydrophilicity of the different bionanocomposite films. As
358 the contact angle kept changing during the sessile measurement, both values at 0 s and 60 s (θ_{c0s} and
359 θ_{c60s}) were recorded. The θ_{c0s} and θ_{c60s} values for A-F were 90±5° and 68±5°, respectively [24]. In
360 comparison, A/M-F had higher contact angle values (θ_{c0s} = 98±6° and θ_{c60s} = 89±6°). Compared with
361 B-F (θ_{c0s} = 71±6°and θ_{c60s} = 60±65°), B/M-F also displayed higher θ_{c0s} (88±6°) and θ_{c60s} (70±11°).
362 These results highlight the effect of inclusion of MMT in enhancing the surface hydrophilicity of
363 both un-plasticised A- and B-matrices, behaviour attributed to the effective biopolymer–MMT
364 interactions and the shielding provided by MMT nanosheets against water molecules.
365

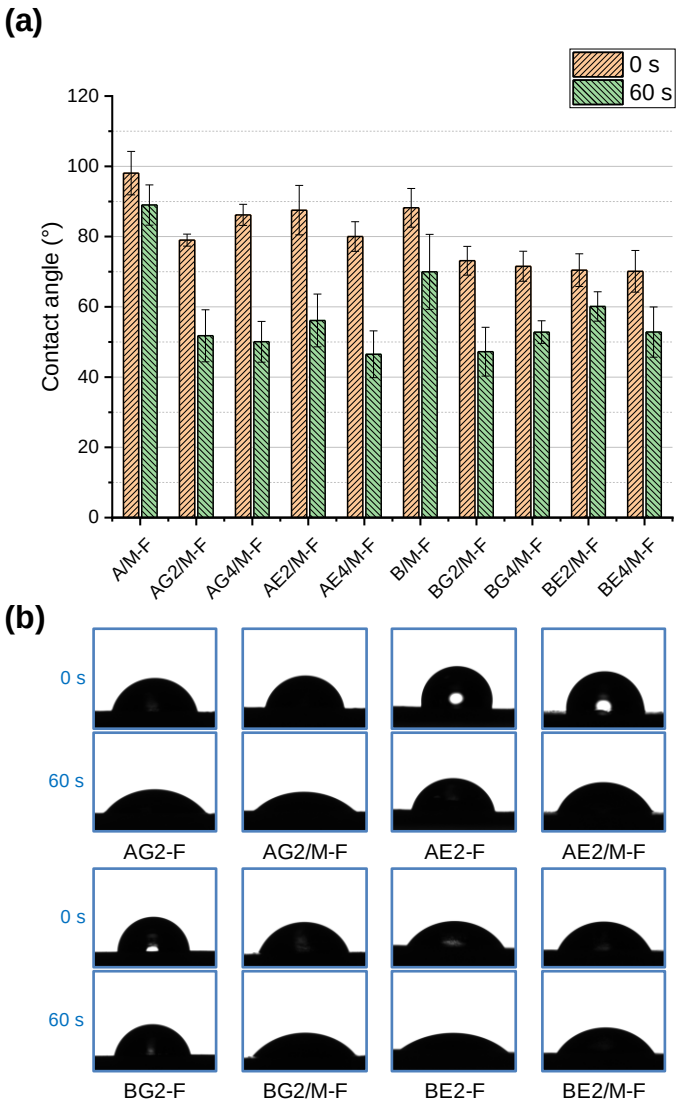

Figure 7. a) Contact angle values and b) droplet images for the different bionanocomposite films at 0 s and 60 s. Error bars represent standard deviations. AG2-F, AE2-F, BG2-F, and BE2-F were tested in our previous studies [25, 26].

For the A-matrix plasticised by glycerol, the surface hydrophilicity only varied with glycerol content but was not affected by inclusion of MMT. Interestingly, BG2-F displayed significantly higher contact angle (θ_{c0s} = 90±6° and θ_{c60s} = 73±8°) than AG2-F (θ_{c0s} = 80±7° and θ_{c60s} = 49±7°) [25], while B-F displayed lower θ_{c0s} and θ_{c60s} than A-F [24]. Nonetheless, compared with BG2-F [25], BG2/M-F exhibited significantly higher surface hydrophilicity, with θ_{c0s} = 73±4° and θ_{c60s} =

47±7°, a consequence of the MMT nanosheets disrupting interactions between biopolymer chains and between biopolymer and glycerol. However, the effect of MMT was negligible with a high content (40 wt%) of glycerol in the B-matrix, as reflected by the similar θ_{c0s} and θ_{c60s} values for BG4-F and BG4/M-F.

Inclusion of MMT led to increased surface hydrophilicity for the A-matrix plasticised by [C_2mim][OAc]. In this regard, MMT disrupts the hydrogen bonding between chitosan chains and the interaction between chitosan and the IL, making more polar groups available to interact with water. In contrast, for the IL-plasticised B-matrix, inclusion of MMT resulted in lower surface hydrophilicity (increased hydrophobicity), possibly due to enhanced PEC between biopolymer chains.

3.3 Discussion on surface hydrophilicity/hydrophobicity of chitosan-based composites

Our previous study [24] indicated that compared with A-F, B-F had much higher hydrolytic stability, attributed to PEC between chitosan and CMC. The enhanced structural stability of biopolymers by PEC can be ascribed to ionic bonds (governed by electrostatic attraction, or Coulomb's law) being stronger than hydrogen bonds. However, B-F still showed higher surface hydrophilicity than A-F [24], due to the higher hydrophilicity of CMC.

Surface hydrophilicity of a biopolymer material is largely determined by the surface free energy linked to chemical groups exposed on the material surface. For some biopolymers such as gelatin, the high chain mobility would allow for the burying of polar groups in the bulk phase, making the surface more hydrophobic. However, for polysaccharides such as chitosan, cellulose and starch, hydroxyl groups are located on planar saccharide rings and, consequently, have much less freedom to

rearrange themselves to change the material surface configuration [38]. According to Zhang et al. [39], the contact angle for solution-cast gelatin/starch films decreased from 114 to 72 with increasing starch content from 0 wt% and 100 wt%, indicating that starch has higher surface hydrophilicity than gelatin. However, research [40, 41] suggested that for chitosan/gelatin films (ratio from 100:0 to 0:100, w/w) without crosslinking prepared by solution casting, the contact angle was in the range of 78–90°; blending gelatin in chitosan was found to result in a moderately lower contact angle (higher surface hydrophilicity) and the pure-gelatin film was still more hydrophilic than the pure-chitosan film. In these studies, the difference in contact angle for gelatin might be due to the different ways of sample preparation, which led to different amounts of gelatin polar groups exposed on the surface. In this current work, as only polysaccharides were involved, we consider the surface hydrophilicity to be mainly linked to the availability of polar groups (typically hydroxyl groups) that participate in hydrogen-bonding interactions and the shielding effect due to the presence of the nanofiller, as illustrated schematically in **Figure 8** and discussed more specifically below. As contact angle decreased with time for the chitosan and chitosan/CMC samples, likely, the wetting process, which disrupted hydrogen bonding in the materials, also allowed more polar groups exposed on the surface.

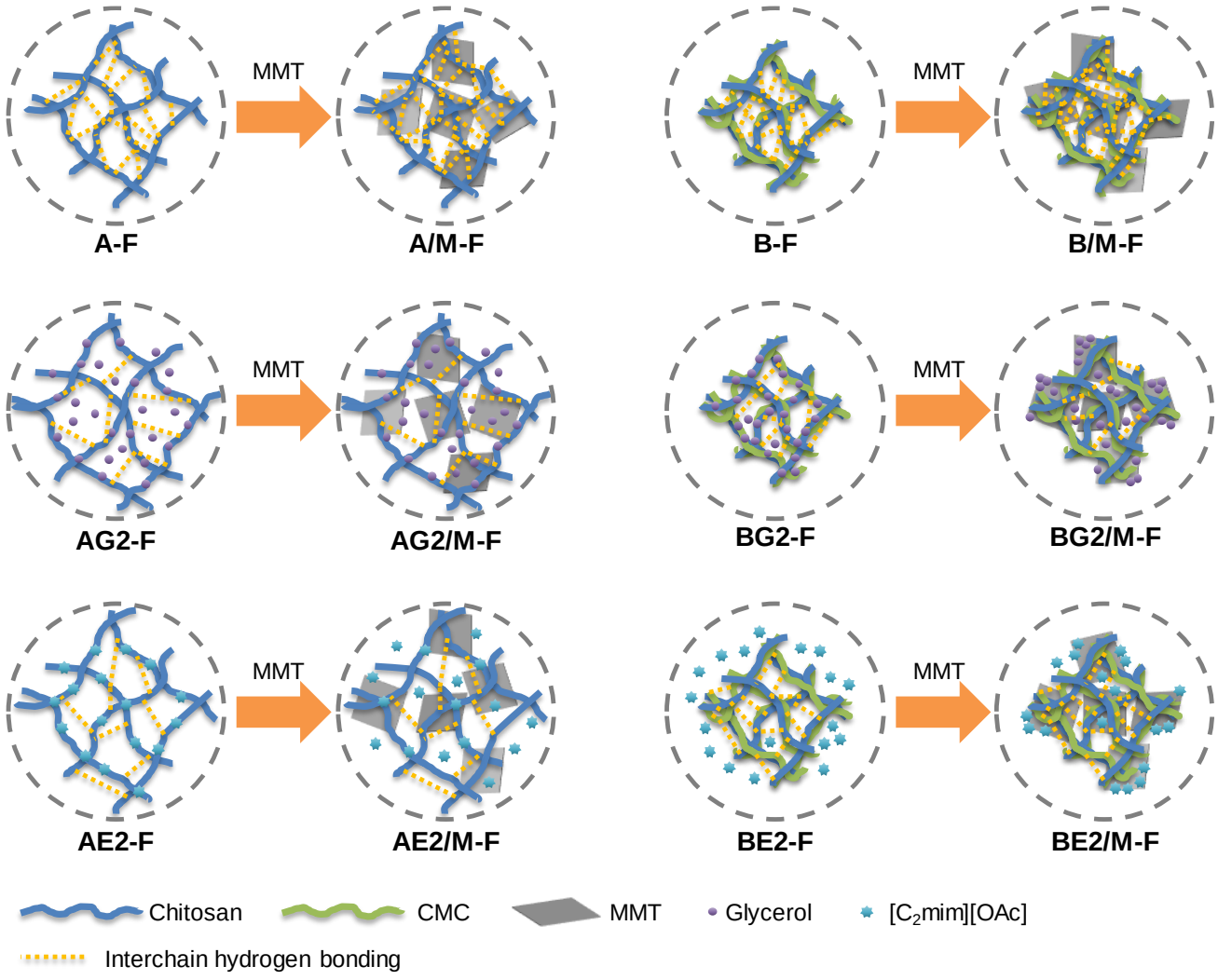

Figure 8. Schematic representation of the structures of the different bionanocomposite films compared to their biopolymer counterparts.

A/M-F and B/M-F had reduced surface wettability relative to A-F and B-F, respectively, as a consequence of the strong hydrogen-bonding and ionic interactions between MMT and chitosan and, the large surface area of MMT nanosheets. Compared with A-F, the A-samples plasticised by glycerol displayed higher surface hydrophilicity. In these samples, glycerol weakened the hydrogen-bonded network in chitosan and increased the biopolymer free volume. Presumably, there was still a significant portion of glycerol molecules not hydrogen-bonded with chitosan polar groups, which

423 could bind with water and contributed to the increased surface hydrophilicity. Due to the more
424 dynamic structure induced by glycerol, inclusion of MMT nanosheets was not effective at shielding
425 the polar groups and reducing the surface hydrophilicity, although it further disrupted the inter-chain
426 hydrogen-bonded network (as shown by reduced E and σ_t).

427 Compared with the glycerol-plasticised A-samples, AE2-F had reduced surface hydrophilicity.
428 In this regard, we propose that the IL anion ($[OAc]^-$) could effectively bind with chitosan hydroxyl
429 and amine groups, significantly reducing the amounts of free hydroxyl and amine groups available
430 for interaction with water. Similarly, Sankri et al. [6] indicated that starch plasticised by $[C_4mim]Cl$
431 were significantly less hygroscopic than the glycerol-plasticised counterpart. Chen et al. [11]
432 suggested that ILs, due to their strong hydrogen-bonding capability, might bind with multiple
433 hydroxyl groups of chitosan. However, the similar mechanical properties of AG2-F and AE2-F [25,
434 26] indicates the formation of substantive hydrogen-bonding crosslinks by $[C_2mim][OAc]$ between
435 chitosan chains was unlikely. Moreover, compared with that of AE2-F, the enhanced surface
436 wettability of AE2/M-F suggests the MMT nanosheets may have restricted binding between the IL
437 and chitosan polar groups.

438 Surprisingly, B/G2-F had low surface hydrophilicity similar to B/M-F. PEC brings the
439 biopolymer chains closer, reducing free volume and assisting the binding between glycerol and
440 biopolymer polar groups, reducing the amounts of free polar groups. Our visual observation indicates
441 that the B-series of samples contracted more than the A-series of samples during conditioning,
442 leading to a denser structure for the former. In agreement with this, a previous study [42] showed the
443 excellent oil and water barrier properties of polyelectrolyte-complexed chitosan/CMC materials,

444 which the authors ascribed to the more dense material structure formed by PEC. PEC-induced
445 densification of chitosan/fibroin materials has also been observed previously [43]. Compared with
446 BG2-F, BG2/M-F displayed increased surface hydrophilicity. In this regard, the competing
447 interactions between glycerol and MMT resulted in a greater amount of free biopolymer polar
448 groups.

449 Unlike AE2-F, BE2-F had high surface wettability. In BE2-F, the IL assisted chain mobility, re-
450 crystallisation, and the interactions between chitosan and CMC (resulting in high thermal stability
451 and T_{α}). However, the interactions between chitosan and CMC also led to more free IL ions that were
452 not interacting with the biopolymers in sample BE2-F. The MMT added could interact with the IL
453 and, thus, reduced surface wettability resulted.

454 4 Conclusions

455 This study shows the different ways in which MMT nanosheets influence the properties of
456 biopolymers, dependent on plasticiser type. For un-plasticised A- and B-matrices, inclusion of MMT
457 largely increased molecular relaxation temperatures, enhanced tensile mechanical properties, and
458 increased surface hydrophobicity, all associated with strong hydrogen bonding and ionic interactions
459 between MMT and chitosan. In particular, MMT shields the biopolymer polar groups, leading to
460 reduced surface hydrophilicity. Meanwhile, inclusion of MMT reduced thermal stability and
461 crystallinity, by hindering biopolymer chain interactions (hydrogen-bonding and/or ionic). When
462 plasticisers such as glycerol or [C_2mim][OAc] are introduced to the biopolymer system, any effect of
463 MMT on material properties largely depends on whether the MMT alters the role of the plasticiser.

Unexpectedly, hydrophilic plasticisers may reduce the surface hydrophilicity of biopolymer films by interacting with biopolymer polar groups. This includes AE2-F, whose high surface hydrophobicity is derived from the strong hydrogen-bonding capability of [C_2mim][OAc], and BG2-F, where PEC assisted the binding between biopolymer polar groups and glycerol. In these cases, inclusion of MMT interrupts the interactions between the plasticiser and biopolymer(s), leading to increased surface wettability, while its effect on the biopolymer inter-chain interactions was marginal. Thus, we conclude the plasticisers and MMT nanosheets influenced the surface hydrophilicity of biopolymer materials mainly by varying the availability of free polar groups of biopolymers.

This study has enabled a better understanding of the structure–property relationships of biopolymers and provided insights into the design of biopolymer materials with tailored hydrophilicity/hydrophobicity for specific applications (*e.g.* packaging, coating, controlled release, wound dressing, and tissue engineering).

Conflicts of Interests

Declarations of interest: none

Acknowledgements

This project has received funding from the European Union's Horizon 2020 research and innovation programme under the Marie Skłodowska-Curie grant agreement No. 798225. P. Chen acknowledges the financial support from the China Scholarship Council (CSC) for her visiting

position and thanks IINM, WMG, University of Warwick, UK for hosting her research visit. F. Xie also acknowledges support from the Guangxi Key Laboratory for Polysaccharide Materials and Modification, Guangxi University for Nationalities, China (Grant No. GXPSMM18ZD-02).

Data availability

The raw/processed data required to reproduce these findings cannot be shared at this time due to technical or time limitations.

References

[1] M.G.A. Vieira, M.A. da Silva, L.O. dos Santos, M.M. Beppu, Natural-based plasticizers and biopolymer films: A review, Eur. Polym. J. 47(3) (2011) 254-263.

[2] F. Xie, B.M. Flanagan, M. Li, P. Sangwan, R.W. Truss, P.J. Halley, E.V. Strounina, A.K. Whittaker, M.J. Gidley, K.M. Dean, J.L. Shamshina, R.D. Rogers, T. McNally, Characteristics of starch-based films plasticised by glycerol and by the ionic liquid 1-ethyl-3-methylimidazolium acetate: A comparative study, Carbohydr. Polym. 111 (2014) 841-848.

[3] F. Xie, B.M. Flanagan, M. Li, R.W. Truss, P.J. Halley, M.J. Gidley, T. McNally, J.L. Shamshina, R.D. Rogers, Characteristics of starch-based films with different amylose contents plasticised by 1-ethyl-3-methylimidazolium acetate, Carbohydr. Polym. 122 (2015) 160-168.

[4] B. Zhang, F. Xie, T. Zhang, L. Chen, X. Li, R.W. Truss, P.J. Halley, J.L. Shamshina, T. McNally, R.D. Rogers, Different characteristic effects of ageing on starch-based films plasticised by 1-ethyl-3-methylimidazolium acetate and by glycerol, Carbohydr. Polym. 146 (2016) 67-79.

503 [5] B. Zhang, F. Xie, J.L. Shamshina, R.D. Rogers, T. McNally, D.K. Wang, P.J. Halley, R.W.
504 Truss, S. Zhao, L. Chen, Facile Preparation of Starch-Based Electroconductive Films with Ionic
505 Liquid, ACS Sustainable Chem. Eng. 5(6) (2017) 5457-5467.
506 [6] A. Sankri, A. Arhaliass, I. Dez, A.C. Gaumont, Y. Grohens, D. Lourdin, I. Pillin, A. Rolland-
507 Sabaté, E. Leroy, Thermoplastic starch plasticized by an ionic liquid, Carbohydr. Polym. 82(2)
508 (2010) 256-263.
509 [7] E. Leroy, P. Jacquet, G. Coativy, A.l. Reguerre, D. Lourdin, Compatibilization of starch–zein
510 melt processed blends by an ionic liquid used as plasticizer, Carbohydr. Polym. 89(3) (2012) 955-
511 963.
512 [8] G. Colomines, P. Decaen, D. Lourdin, E. Leroy, Biofriendly ionic liquids for starch
513 plasticization: a screening approach, RSC Advances 6(93) (2016) 90331-90337.
514 [9] P. Decaen, A. Rolland-Sabaté, S. Guilois, V. Jury, N. Allanic, G. Colomines, D. Lourdin, E.
515 Leroy, Choline chloride vs choline ionic liquids for starch thermoplasticization, Carbohydr. Polym.
516 177(Supplement C) (2017) 424-432.
517 [10] F. Ren, J. Wang, F. Xie, K. Zan, S. Wang, S. Wang, Applications of ionic liquids in starch
518 chemistry: a review, Green Chem. 22(7) (2020) 2162-2183.
519 [11] M. Chen, T. Runge, L. Wang, R. Li, J. Feng, X.-L. Shu, Q.-S. Shi, Hydrogen bonding impact on
520 chitosan plasticization, Carbohydr. Polym. 200 (2018) 115-121.
521 [12] L.F. Boesel, Effect of plasticizers on the barrier and mechanical properties of biomimetic
522 composites of chitosan and clay, Carbohydr. Polym. 115 (2015) 356-363.

523 [13] B. Ates, S. Koytepe, A. Ulu, C. Gurses, V.K. Thakur, Chemistry, Structures, and Advanced
524 Applications of Nanocomposites from Biorenewable Resources, Chem. Rev. 120(17) (2020) 9304-
525 9362.
526 [14] F. Xie, E. Pollet, P.J. Halley, L. Avérous, Starch-based nano-biocomposites, Prog. Polym. Sci.
527 38(10-11) (2013) 1590-1628.
528 [15] P. Kampeerapappun, D. Aht-ong, D. Pentrakoon, K. Srikulkit, Preparation of cassava
529 starch/montmorillonite composite film, Carbohydr. Polym. 67(2) (2007) 155-163.
530 [16] K. Wilpiszewska, A.K. Antosik, T. Spychaj, Novel hydrophilic carboxymethyl
531 starch/montmorillonite nanocomposite films, Carbohydr. Polym. 128 (2015) 82-89.
532 [17] D.F. Xie, V.P. Martino, P. Sangwan, C. Way, G.A. Cash, E. Pollet, K.M. Dean, P.J. Halley, L.
533 Avérous, Elaboration and properties of plasticised chitosan-based exfoliated nano-biocomposites,
534 Polymer 54(14) (2013) 3654-3662.
535 [18] V. Epure, M. Griffon, E. Pollet, L. Avérous, Structure and properties of glycerol-plasticized
536 chitosan obtained by mechanical kneading, Carbohydr. Polym. 83(2) (2011) 947-952.
537 [19] M. Matet, M.-C. Heuzey, E. Pollet, A. Ajji, L. Avérous, Innovative thermoplastic chitosan
538 obtained by thermo-mechanical mixing with polyol plasticizers, Carbohydr. Polym. 95(1) (2013)
539 241-251.
540 [20] C. Gao, E. Pollet, L. Avérous, Properties of glycerol-plasticized alginate films obtained by
541 thermo-mechanical mixing, Food Hydrocolloids 63 (2017) 414-420.
542 [21] C. Gao, E. Pollet, L. Avérous, Innovative plasticized alginate obtained by thermo-mechanical
543 mixing: Effect of different biobased polyols systems, Carbohydr. Polym. 157 (2017) 669-676.

544 [22] K. Murakawa, D.R. King, T. Sun, H. Guo, T. Kurokawa, J.P. Gong, Polyelectrolyte
545 complexation via viscoelastic phase separation results in tough and self-recovering porous hydrogels,
546 J. Mater. Chem. A 7(35) (2019) 5296-5305.
547 [23] P. Chen, F. Xie, F. Tang, T. McNally, Structure and properties of thermomechanically
548 processed silk peptide and nanoclay filled chitosan, Nanocomposites 6(3) (2020) 125-136.
549 [24] P. Chen, F. Xie, F. Tang, T. McNally, Thermomechanical-induced polyelectrolyte complexation
550 between chitosan and carboxymethyl cellulose enabling unexpected hydrolytic stability, Compos.
551 Sci. Technol. 189 (2020) 108031.
552 [25] P. Chen, F. Xie, F. Tang, T. McNally, Glycerol plasticisation of chitosan/carboxymethyl
553 cellulose composites: Role of interactions in determining structure and properties, Int. J. Biol.
554 Macromol. 163 (2020) 683-693.
555 [26] P. Chen, F. Xie, F. Tang, T. McNally, Ionic Liquid (1-Ethyl-3-methylimidazolium Acetate)
556 Plasticization of Chitosan-Based Bionanocomposites, ACS Omega 5(30) (2020) 19070-19081.
557 [27] P. Chen, F. Xie, F. Tang, T. McNally, Structure and properties of thermomechanically
558 processed chitosan/carboxymethyl cellulose/graphene oxide polyelectrolyte complexed
559 bionanocomposites, Int. J. Biol. Macromol. 158 (2020) 420-429.
560 [28] F. Chivrac, E. Pollet, M. Schmutz, L. Avérous, New approach to elaborate exfoliated starch-
561 based nanobiocomposites, Biomacromolecules 9(3) (2008) 896-900.
562 [29] F. Chivrac, E. Pollet, M. Schmutz, L. Avérous, Starch nano-biocomposites based on needle-like
563 sepiolite clays, Carbohydr. Polym. 80(1) (2010) 145-153.

564 [30] S.F. Wang, L. Shen, Y.J. Tong, L. Chen, I.Y. Phang, P.Q. Lim, T.X. Liu, Biopolymer
565 chitosan/montmorillonite nanocomposites: Preparation and characterization, Polym. Degrad. Stab.
566 90(1) (2005) 123-131.
567 [31] A. Ahmed, Y. Chaker, E.H. Belarbi, O. Abbas, J.N. Chotard, H.B. Abassi, A.N. Van Nhien, M.
568 El Hadri, S. Bresson, XRD and ATR/FTIR investigations of various montmorillonite clays modified
569 by monocationic and dicationic imidazolium ionic liquids, J. Mol. Struct. 1173 (2018) 653-664.
570 [32] A. Leszczyńska, J. Njuguna, K. Pielichowski, J.R. Banerjee, Polymer/montmorillonite
571 nanocomposites with improved thermal properties: Part II. Thermal stability of montmorillonite
572 nanocomposites based on different polymeric matrixes, Thermochim. Acta 454(1) (2007) 1-22.
573 [33] I. Quijada-Garrido, B. Laterza, J.M. Mazón-Arechederra, J.M. Barrales-Rienda, Characteristic
574 Features of Chitosan/Glycerol Blends Dynamics, Macromol. Chem. Phys. 207(19) (2006) 1742-
575 1751.
576 [34] I. Quijada-Garrido, V. Iglesias-González, J.M. Mazón-Arechederra, J.M. Barrales-Rienda, The
577 role played by the interactions of small molecules with chitosan and their transition temperatures.
578 Glass-forming liquids: 1,2,3-Propantriol (glycerol), Carbohydr. Polym. 68(1) (2007) 173-186.
579 [35] M.S. Kim, G. Khang, H.B. Lee, Gradient polymer surfaces for biomedical applications, Prog.
580 Polym. Sci. 33(1) (2008) 138-164.
581 [36] P.B. van Wachem, T. Beugeling, J. Feijen, A. Bantjes, J.P. Detmers, W.G. van Aken,
582 Interaction of cultured human endothelial cells with polymeric surfaces of different wettabilities,
583 Biomaterials 6(6) (1985) 403-408.

584 [37] T. Mohan, R. Kargl, K.E. Tradt, M.R. Kulterer, M. Braćić, S. Hribernik, K. Stana-Kleinschek,
585 V. Ribitsch, Antifouling coating of cellulose acetate thin films with polysaccharide multilayers,
586 Carbohydr. Polym. 116 (2015) 149-158.
587 [38] H. Yasuda, A.K. Sharma, T. Yasuda, Effect of orientation and mobility of polymer molecules at
588 surfaces on contact angle and its hysteresis, Journal of Polymer Science: Polymer Physics Edition
589 19(9) (1981) 1285-1291.
590 [39] N. Zhang, H. Liu, L. Yu, X. Liu, L. Zhang, L. Chen, R. Shanks, Developing gelatin–starch
591 blends for use as capsule materials, Carbohydr. Polym. 92(1) (2013) 455-461.
592 [40] V. Chiono, E. Pulieri, G. Vozzi, G. Ciardelli, A. Ahluwalia, P. Giusti, Genipin-crosslinked
593 chitosan/gelatin blends for biomedical applications, J. Mater. Sci.: Mater. Med. 19(2) (2008) 889-
594 898.
595 [41] E. Pulieri, V. Chiono, G. Ciardelli, G. Vozzi, A. Ahluwalia, C. Domenici, F. Vozzi, P. Giusti,
596 Chitosan/gelatin blends for biomedical applications, Journal of Biomedical Materials Research Part
597 A 86A(2) (2008) 311-322.
598 [42] S. Basu, A. Plucinski, J.M. Catchmark, Sustainable barrier materials based on polysaccharide
599 polyelectrolyte complexes, Green Chem. 19(17) (2017) 4080-4092.
600 [43] L. Meng, F. Xie, B. Zhang, D.K. Wang, L. Yu, Natural Biopolymer Alloys with Superior
601 Mechanical Properties, ACS Sustainable Chem. Eng. 7(2) (2019) 2792-2802.
602

§ Supporting Information §

Influence of plasticizer type and nanoclay on the properties of chitosan-based materials

Pei Chen [a,b], Fengwei Xie [b,*,†], Fengzai Tang [c], Tony McNally [b,**]

[a] *College of Food Science, South China Agricultural University, Guangzhou, Guangdong 510642, China*

[b] *International Institute for Nanocomposites Manufacturing (IINM), WMG, University of Warwick, Coventry CV4 7AL, United Kingdom*

[c] *WMG, University of Warwick, Coventry CV4 7AL, United Kingdom*

[*] Corresponding author. Email addresses: d.xie.2@warwick.ac.uk, fwhsieh@gmail.com (F. Xie)

[**] Corresponding author. Email address: t.mcnally@warwick.ac.uk (T. McNally)

[†] This author leads the research.

1 Figures

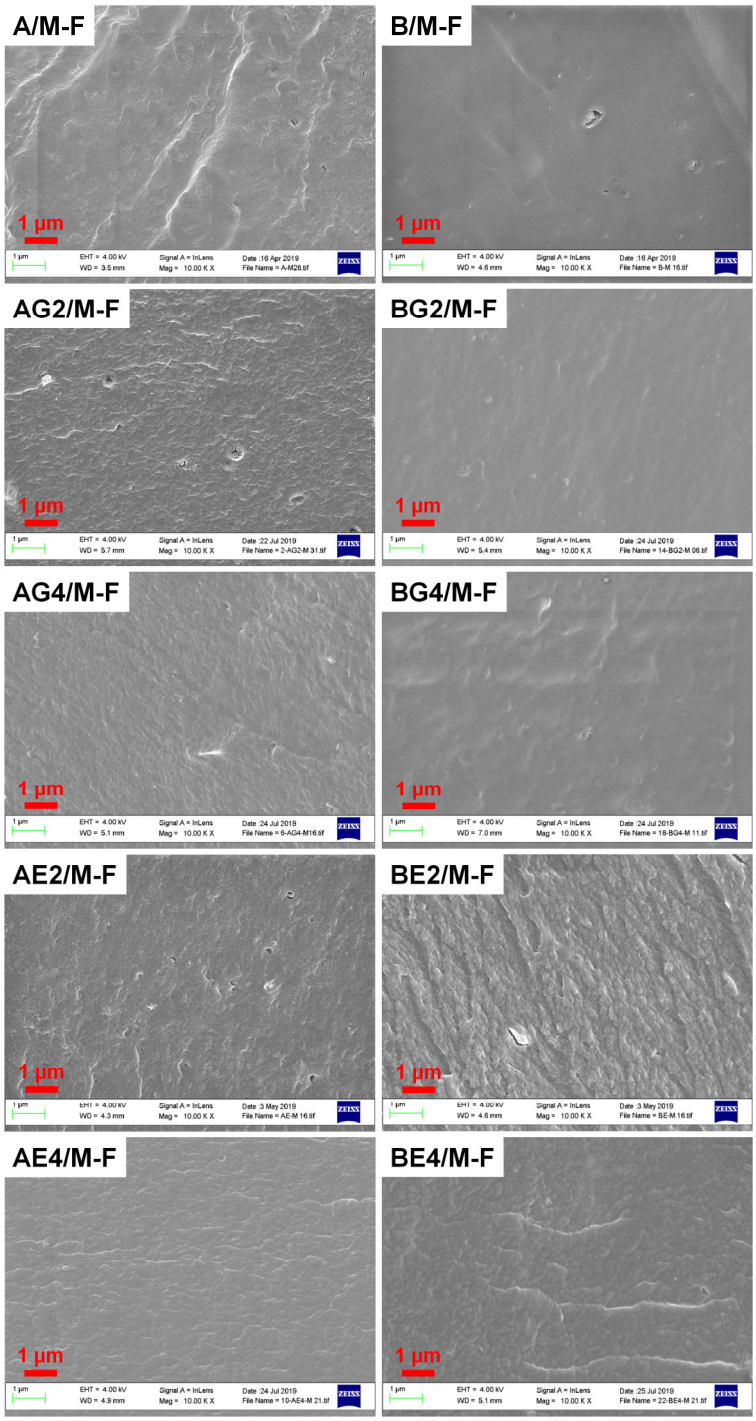

Figure S1. Scanning electron microscopy (SEM) images of cryofractured surfaces of the different bionanocomposite films.

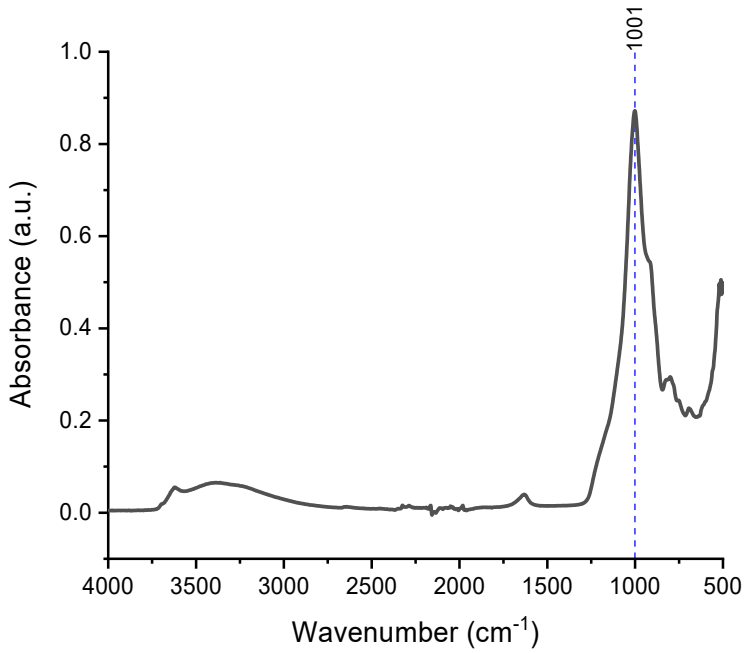

Figure S2. Fourier-transform infrared (FTIR) spectrum of montmorillonite (MMT).

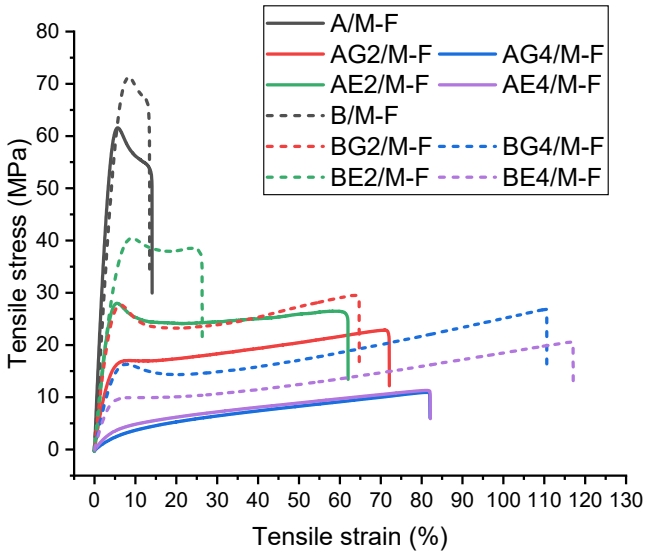

Figure S3. Representative stress–strain curves under tensile testing for the different bionanocomposite films.